IEEE Photonics Journal
An IEEE Photonics Society Publication

Photobleaching-Insensitive Fluorescence Diagnostics in Skin and Brain Tissue

Volume 3, Number 3, June 2011

M. Brydegaard
N. Haj-Hosseini
K. Wårdell
S. Andersson-Engels

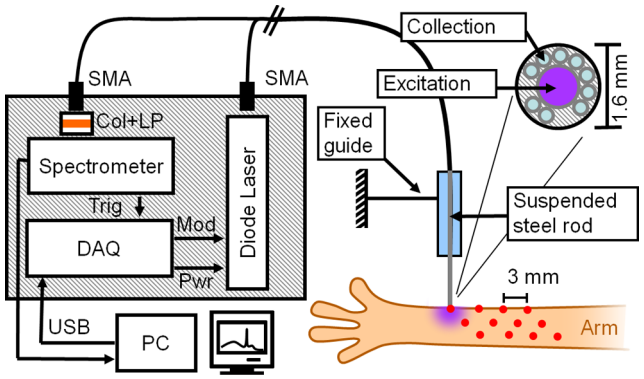

DOI: 10.1109/JPHOT.2011.2141656
1943-0655/$26.00 ©2011 IEEE

IEEE photonics SOCIETY

IEEE

Photobleaching-Insensitive Fluorescence Diagnostics in Skin and Brain Tissue

M. Brydegaard,[1] N. Haj-Hosseini,[2] K. Wårdell,[2] and S. Andersson-Engels[1]

[1]Department of Physics, Lund University, 221 00 Lund, Sweden
[2]Department of Biomedical Engineering, Linköping University, 581 85 Linköping, Sweden

DOI: 10.1109/JPHOT.2011.2141656
1943-0655/$26.00 ©2011 IEEE

Manuscript received March 1, 2011; revised April 3, 2011; accepted April 5, 2011. Date of publication April 11, 2011; date of current version May 6, 2011. This work was supported by a Swedish Research Council (VR) Linnaeus grant to the Lund Laser Center (LLC), the Swedish Foundation for Strategic Research (SSF), the VR Group under Grant No. 331-2006-7661, and a PIEp/IDRE Swedish innovation initiative grant. Corresponding author: M. Brydegaard (e-mail: Mikkel.Brydegaard@fysik.lth.se).

Abstract: In this paper, we investigate the possibility of using accurate prediction models for the prediction of protoporphyrin bleaching dynamics to achieve photobleaching-insensitive methods to improve the evaluation of data in an existing clinical fluorescence-guided resection technique. To simulate the scenario, measurements were carried out *in vivo* on skin of healthy volunteers using a compact fiber-based fluorescence spectroscopy system. We have developed an effective method for the parameterization of sequences of bleaching spectra. We analyze convergence and decay rates with respect to initial conditions and excitation irradiance. We also discuss the consequences and the potential for bleaching-insensitive measurements and their applicability in a few examples from *in vivo* open brain surgery.

Index Terms: Fluorescence-guided resection, FGR, 5-ALA, PpIX, protoporphyrin, photobleaching, laser-induced fluorescence spectroscopy, LIF, optical diagnostics, tissue optics, skin, brain, dynamic models, system identification, state space models.

1. Introduction

1.1. Background of Fluorescence-Guided Resection

Optical diagnostic methods are important tools in modern medicine due to their often noninvasive nature and due to their rapid evaluation possibilities [1]. In the area of open brain surgery, two such types of fluorescence-based methods are currently being developed to assist the surgeon in deciding which tissue to remove and which to spare. Both methods rely on the increased concentration of fluorescent tumor markers, e.g., protoporphyrin (PpIX) [2]–[7], in malignant tumors. Imaging systems incorporated into the surgeon's stereo microscope have been developed, in which the fluorescence intensity can be displayed in every point at the line of sight in the area of resection [8]–[10]. However, these types of methods have limited depth penetrating ability, and their use is restricted in subsurface regions or regions covered by fluids such as blood or flushing liquid. Another kind of method consists of a nonimaging, contact-point fiber probe [11]–[13] (see Fig. 1), allowing the surgeon to penetrate tumor tissue with the probe tip and proceed to underlying regions when the signal from the instrument confirms the presence of the tumor. These methods provide comparably extended depth information. The brain surgeon's task is extremely demanding, and any tool that can provide aid without causing additional concern or distraction is welcome. In terms of performance, both imaging and contact-fiber probe systems have advantages and disadvantages. Imaging systems

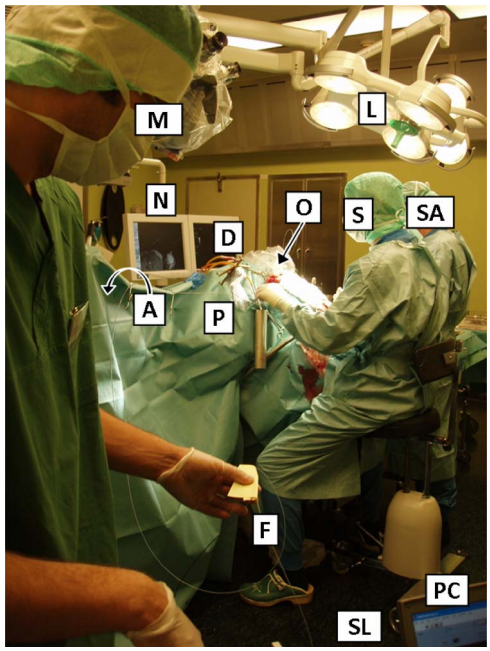

Fig. 1. Scene in the operation theater, demonstrating *in vivo* measurements during open brain surgery. (P) Patient, (S) surgeon, (SA) surgeon's assistant, (O) skull opening, (A) anesthetist and surveillance monitors, (L) surgical light system, (M) operating microscope, (N) displays showing offline MRI maps and navigation system, (D) flushing/ultrasonic tool drainage tubes, (F) fiber probe, (SL) box containing the spectrometer and laser, and (PC) controlling laptop.

are integrated into the operating microscope, while the steel rod fiber probe can be combined with the additional hand tools used by the surgeon, such as ultrasonic vacuum suction devices, scalpels, and navigation systems [14]. Both imaging and fiber-based systems must be compatible with the bright spotlights used in the operation theater (see Fig. 1). Further, the instruments have to be compatible with sterilization procedures. However, both types of systems suffer from the fact that the measurement of PpIX concentration influences the concentration itself due to photobleaching [15]–[23]. This can lead to inconsistency in the measurements. In a typical situation, in which the ratio between the PpIX and the tissue autofluorescence is used to determine whether to remove brain tissue or not, the criterion for removal might be met in one instance, while after bleaching, just a few seconds later, it might not be met in the same region. In this paper, we have investigated the possibility of improving the evaluation of a clinically used fiber-based method to achieve bleaching-insensitive methods. We used *in vivo* healthy skin measurements as a model for the process in a manner which resembles the actual clinical scenario. We then tested the applicability on a limited set of *in vivo* brain tumor data acquired during open brain surgery.

1.2. Dynamic Modeling

In the fluorescence measurements performed in this paper, the recorded fluorescence spectrum will depend on the fluorophore concentration in a complex way. First, we will develop a dynamic model to describe the evolution of the fluorescence spectrum when recording the fluorescence over a period of time from the same tissue location. This model describes the photobleaching process of the involved chromophores. Our ambition in this paper is to learn whether such dynamic model can be used to improve the consistency of the criterion for tissue resection under severe bleaching conditions. When light from the excitation fiber impinges on the tissue, it undergoes photomigration, and the energy is deposited in the interrogation volume in a manner governed by the absorption coefficients and scattering properties of the sample at the excitation wavelength [1]. The total absorption is the sum of all the absorbing constituent concentrations multiplied by their respective

absorption cross sections. The absorbed energy is then partly turned into heat, partly reemitted as fluorescence, and partly consumed to drive photochemically induced reactions. The last mentioned pathway can in turn lead to destruction of the particular molecules, which would alter the local absorption coefficient. This, in turn, will result in a change in the extension of the interrogation volume and the volume in which the excitation energy is deposited with time in a sequence of measurements. When a bleachable sensitizer is embedded in a presumably nonbleachable tissue matrix [24], this may lead to an increase in autofluorescence over time as the sensitizer bleaches out of the interrogation volume, hence quenching the excitation and emission of the autofluorescence to a lesser degree. This is known to have only a small effect on the tissue autofluorescence, but some studies suggest that autofluorescence increases during bleaching, e.g., [17], and another suggests a decrease [3], [24].

The fluorescent light emitted from each volume element eventually undergoes a second photon migration process and may be subject to emission quenching or re-absorption before reaching the detection fiber. The detected spectrum is thus perturbed by any absorber present within the emitted spectral range within the interrogation volume. To evaluate the spectral shape of the recorded fluorescence spectra, data can be reduced from the number of spectral bands in the spectrometer to the number of spectral components involved by using singular value decomposition (SVD, which is identical to principal component analysis (PCA), except that the mean is not subtracted in SVD) [25]–[30]. When decomposing the spectra from such a bleaching sequence with SVD, a truncation point can be determined from the spectral eigenvalues. The spectrum at any given time in the sequence can be described by a linear combination of the corresponding eigenvectors or base spectra. The loadings related to the concentrations of the involved substances (and, thus, their respective cross sections) can be expected to perturb the interrogation volume and the energy deposition; thus, the loadings can be considered as dynamical states. In the mathematical space defined by the concentration loadings, the time-evolution trajectory resulting from a bleaching sequence can be expected to be governed by a certain function of the concentration composition in the previous instance. Such trajectories can thus be described by a vector field, which can be obtained by performing system identification [31]–[36]. While we can expect at least as many dynamic states in the dynamic model as linearly independent base spectra, we cannot exclude the possibility of more hidden dynamic states. It is, however, generally accepted that the bleaching process of PpIX in tissue can be fairly well described by two dynamic states [24], [37]. Each absorber can either remain stable, be destroyed and go to a nonabsorbing state (increasing the fluorescence from deeper lying fluorophores), go to a nonfluorescing state, or turn into a new compound influencing the detected fluorescence in a new way [22], [37], [38]. All such behaviors are included in state space models used in control theory and robotics, the evolution of ecosystems, and chemical and nuclear chain decays [31]–[36]. Here, the dynamic states are expressed as a linear combination (the so-called system matrix or dynamic model) of the same dynamic states in the previous instance or instances. The diagonal elements of the system matrix correspond to individual exponential decays, whereas the coefficients off the diagonal represent the production or destruction of one dynamic state related to another dynamic state. While the tissue autofluorescence obviously does not bleach to a nonzero value within a reasonable time, it is less intuitive that the sensitizer concentration bleaches to anything else than to zero. However, several indications point toward such a behavior [39], [40]. Reasons for this behavior might be found in the bottleneck of dissolved oxygen in-flow to the interrogation volume, in diffusion into or production of PpIX inside the interrogation volume [41]. Other reasons may be found in the fact that the PpIX sensitizer can be found in different subcellular compartments with different ambient conditions, and bleaching only takes place in the simultaneous presence of dissolved oxygen and PpIX [42]. There are also indications of a fluorescent photoproduct from the destruction of PpIX [22], [37], [38], [41], [42].

While the concentration composition constantly changes along the trajectory in the state space [34], a few properties of such a trajectory remains constant and could hence be used for photobleaching-insensitive evaluation. These properties include the convergence composition point, which is reached either by solving the zero derivatives of the transfer function, or to extrapolating bleaching to infinity. The system dynamics and decay times found in the coefficients in

the system matrix of a state space model are also constant throughout the bleaching process. If any of these properties depends on the initial concentration composition, a bleaching-insensitive method could be achieved by applying dynamic models to the short bleaching sequences. Apart from the time-invariant transfer function, we can also expect time-dependent behavior in an *in vivo* scenario. Heart beats and breathing [43], [44] may give rise to slight variations in the optical return or diffusion properties, as well as any movement's of the surgeon's hand. Such difficulties could be overcome by optimizing the instrument for fast acquisition, rather than a plurality of spectral bands.

2. Methods and Data Set

2.1. Optical Touch Pointer

We have recently developed and presented a fiber-optic fluorescence spectrometer [13]. The system can be operated in either continuous or a modulated mode (for background subtraction). Excitation is achieved by a near-UV diode laser module emitting at 405 nm with a maximal power of 50 mW (Oxxius, Lannion, France). A spectrometer (EPP 2000, Stellarnet, Tampa, FL, USA) operating in the wavelength range of 240–850 nm with a resolution of 3 nm is coupled to the system to obtain the optical signal. The elastically back-scattered light from the tissue is rejected by a 3-mm long-pass, cutoff filter at 475 nm (Schott CG-GG-475-0.50-3, CVI Melles Griot, Albuquerque, NM, USA). A fiber-optic probe, in contact with the tissue at distal end, is connected to the laser source and the spectrometer. The probe consist of an excitation fiber in the center $(\varnothing_{\text{core}} = 600\ \mu\text{m}, \text{NA} = 0.37$ in air$)$ surrounded by nine collection fibers $(\varnothing_{\text{core}} = 200\ \mu\text{m}, \text{NA} = 0.22$ in air$)$. The technical description of the system and the method of use have been presented previously [13]. The modulation of the laser is synchronized by the spectrometer read out using the counter circuit in the data acquisition board (National Instruments, Inc., Austin, TX, USA).

2.2. Skin Measurements

The measurements were performed on four volunteers after obtaining permission from the local ethical committee (No. M139-07, and No. T83-09, *Regionala etikprövningsnämnden i Linköping*). Written informed consent was obtained from all participants. Methylaminolevulinat cream (METVIX® 160 mg/g, Photocure ASA, Norway) was applied topically in a 2–3-mm-thick layer over an area of roughly 3 cm^2 on the tape-stripped skin of the forearm, 4–6 hours prior to the measurements. The pharmacokinetics of PpIX is described in several studies [38], [45]–[49], and within the given time, the levels can be assumed saturated. During this interval the treated site was covered by a nontransparent plaster to avoid any light exposure. The arm was fixed, and the measurements were performed about 3 mm apart [see Fig. 2(a)] on a new site for each sequence. The probe was suspended in a gliding guide tube and the pressure on the skin can be assumed constant between sequences and test persons. The sequences were recorded in a darkened room. However, in between the measurements, the light was turned on.

The laser was adjusted to fiber tip continuous powers of 1, 2.5, 5, 7.5, and 10 mW (the average power for the modulated measurements is half that of the continuous ones). The irradiation was administered to an area of 0.28 mm^2. In each measurement the recording was made until the PpIX peak at 635 nm was substantially photobleached [see Fig. 2(b)]. In some measurements, specifically those at higher laser power, the measurement was stopped earlier due to irritation of the skin. The integration time of the spectrometer was 200 ms, in continuous mode, and 100 ms, in the modulated mode, which was matched to the duration of laser-on/off time slots. In modulated mode, the sum of two consecutive spectra were stored. Thus, the sampling rate for continuous acquisition was 200 ms, and for modulated sequences, it was 400 ms since dark spectra were continuously recorded in the 1–0 ms laser off-time slots. Recordings were performed on both nontreated and ALA-treated skin on four individuals. In total, 129 sequences were recorded on ALA-treated skin were recorded, out of which 44 were in modulated mode and 85 in continuous mode. Further, 90 sequences were also recorded on nontreated skin, including 30 recorded in modulated mode and 60 in continuous mode.

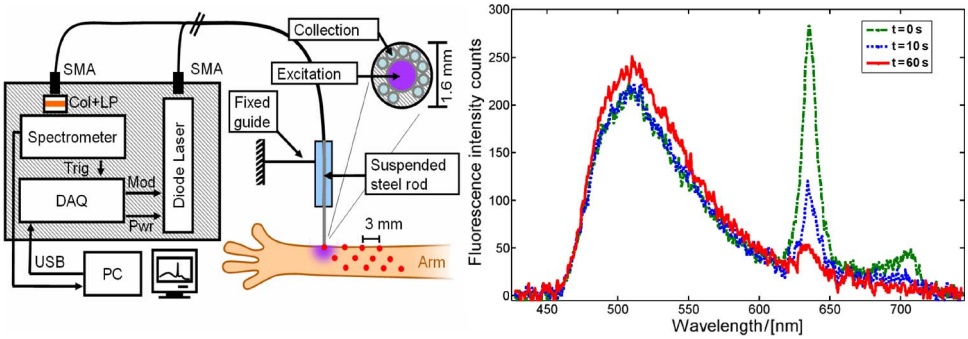

Fig. 2. (Left) Apparatus used to measure laser-induced fluorescence. (Right) Example of bleaching of ALA-treated skin excited by 7.5 mW of continuous 405-nm light. The green light distribution around 500 nm arises due to the tissue autofluorescence and increases slightly with time in this case. The red fluorescence at 635 nm arises from the photosensitizer, i.e., PpIX, and decreases with time of radiation. The signal is considerably different from those obtained in imaging systems due to photon migration [10].

2.3. Brain Measurements

The applicability of the method to a few examples of *in vivo* brain fluorescence measurement (Ethical Committee, No. M139-07) is also presented in this paper. ALA, 5 mg/kg diluted in orange juice, was administered orally approximately 3–4 hours before the measurements were initiated. Five sequences were recorded from the brain tumor tissue during tumor resection surgery, all from the same patient. The tumor was suspected to be a glioblastoma multiforme. Three of these recordings were performed in continuous mode in full operation theater light but with a shielding device covering the tissue in an approximately 10-mm vicinity from the probe. Three sequences were recorded in modulated mode with background subtraction. The excitation power was 5 mW and the integration time 500 ms in tumor tissue in both cases.

2.4. Data Processing and Analysis

Sequence data files were imported into Matlab (MathWorks Inc.) [30]. In the case of acquisition with modulated mode, the dark spectra were subtracted; in the case of the continuous mode, the dark current was estimated from the mean of the dark region blocked by the optical long-pass filter. The intensity counts were normalized to the exposure time (constant) and the varying laser powers. Time frames showing continuous bleaching sequences were handpicked after analyzing the total intensity over time. Thus, spectra obtained prior to skin contact and unsteady sequences were excluded. In total, 40 891 spectra were included, belonging to 219 bleaching sequences, including ALA-treated and non-ALA-treated regions, irradiated by different excitation powers. The spectra were organized in a single matrix M, the rows being the individual observations and columns representing the spectral bands. M was decomposed with SVD

$$M_{n=1..N,\lambda} = U_{n=1..N,s=1..N} \Sigma_{n=1..N,s=1..N} V^*_{\lambda,s=1..N}. \quad (1)$$

Here, U is a matrix with rows representing individuals and columns corresponding to the content of each base spectrum. Σ is a diagonal matrix with eigenvalues representing the significance of each base spectrum in decreasing order. V is a matrix with rows representing spectral bands and columns corresponding to spectral components with decreasing significance. By analyzing the eigenvalues in a log scale plot the noise floor and numbers of significant components can be judged, and a truncation tr can be decided; thus, the entire data set can be expressed as

$$\widehat{M}_{n=1..N,\lambda} = U_{n=1..N,s=1..tr} \Sigma_{s=1..tr,s=1..tr} V^*_{\lambda,s=1..tr}. \quad (2)$$

Here, $\widehat{M}$ is the approximated matrix M using a truncated number of base spectra in V. The base spectra in the columns of V might not necessarily have a physical interpretation; we are, however, allowed to freely rotate the first tr components of V without introducing any loss of information, since a rotational matrix has a determinant of one. To give a meaningful name to spectral base components, we may choose to rotate the base vectors in V according to some preknowledge, e.g., spectral features at certain regions or features expected from treated or nontreated samples

$$B_{\lambda,s=1..tr} = R_{s=1..tr,s=1..tr,} V_{\lambda,s=1..tr}. \tag{3}$$

Here, B is a matrix containing new meaningful base spectra in the columns, and R is a rotational matrix with rotational angles based on preknowledge. Quantities of the composition in terms of meaningful components can now be found by projection, that is, minimizing the least-square residual

$$Y_{n=1..N,s=1..tr} = \left(B^T_{\lambda,s=1..tr} B_{\lambda,s=1..tr}\right)^{-1} B^T_{\lambda,s=1..tr} M_{n=1..N,\lambda}. \tag{4}$$

In practice, these compositions can be rapidly calculated using the QR factorization algorithm [30]. If one spectral component can be assumed to be associated with the tissue/matrix autofluorescence, the composition can be normalized by that constituent, and dimensionless concentration-like quantities C are obtained:

$$C_{n=1..N,s=1..tr-1} = \frac{Y_{n=1..N,s=2..tr}}{Y_{n=1..N,s=auto\ matrix}}. \tag{5}$$

Such a dimensionless quantity could be the PpIX ratio typically used for resection criterion. In photokinetics, the spectral composition can be expressed in a sequence $Y_{t,s=1,...,tr}$ or $C_{t,s=1,...,tr}$, which is retrieved from a (possibly changing) interrogation volume as a function of the spectral composition in the previous instance

$$Y_{t,s=1..tr} = Y_{t-1,s=1..tr} \theta_{s=1..tr,s=1..tr}. \tag{6}$$

Here, θ is the system matrix of the dynamic model. The diagonal terms in θ correspond to decay rates of simple single exponential decays. The terms off the diagonal in θ represents the possibility of onecomponent turning into another detectable component. Several impositions can be set on θ regarding strict stability theorems [31]–[35]; for example, the eigenvalues of the system matrix cannot be complex if it is assumed that there are no cycles in the photochemical reaction chain. Since all spectral components must necessarily converge to zero in the above model (seen by solving $Y_t = Y_{t-1}, \theta \neq 1$), it is necessary to add a bias term to allow the model to converge to anything else than zero

$$Y_{t=1..T,s=1...tr} = \Phi_{t=0..T-1,d=1..DOF} \theta_{d=1..DOF,s=1...tr}, \qquad \Phi = [1 \quad Y_{t=0..T-1,s=1...tr}]. \tag{7}$$

DOF are the degrees of freedom in the dynamical model, and in this case, $DOF = tr + 1$. Obviously, such models can be expanded to any degree of complexity, including polynomial expansions and cross products of the columns in Y. They should, however, have a physical interpretation, and additional DOFs imply decreased stability, and poorer convergence, and an increase in the number of observations required to estimate a good model. A rough estimate of the dynamic model coefficients can be found by regression:

$$\hat{\theta}_{d=1..DOF,s=1..tr} = \left(\Phi^T_{t=0..T-1,d=1..DOF} \Phi_{t=0..T-1,d=1..DOF}\right)^{-1} \Phi^T_{t=0..T-1,d=1..DOF} Y_{t=1..T,s=1..tr}. \tag{8}$$

Again, this can be rapidly calculated by the QR factorization. This estimate can be used as an initial guess, and the dynamic model coefficients $\hat{\theta}$ and initial conditions $\widehat{Y}_0$ can be refined by minimizing the

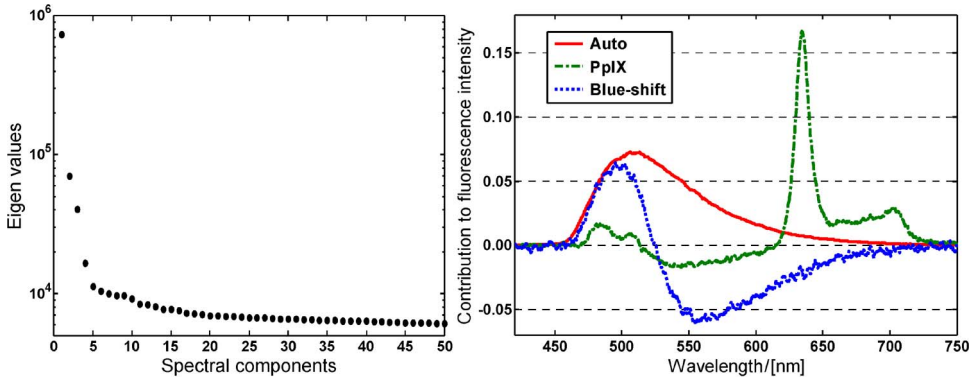

Fig. 3. (Left) Singular value decomposition reveals that all 40 891 spectra can be described as a linear function of four spectra. Note that components beyond the 50th have been omitted. (Right) Base spectra upon which the rest of the analysis is based. The base spectra from the SVD are rotated so that the first principal components match the autofluorescence constructed as the mean spectrum for non-ALA-treated skin.

squared residuals from prediction from time zero

$$\min_{\hat{Y}_0\hat{\theta}}\left(\sum_{t=1..T}\sum_{s=1..tr}\left(Y_{t=1..T,s=1..tr}-\widehat{Y}_{0,s=1..tr}\hat{\theta}^{t=0..T}_{d=1..DOF,s=1..tr}\right)^2\right). \tag{9}$$

In our model, we refined the coefficient iteratively and numerically. The spectral composition at infinity was calculated as

$$\widehat{Y}_{\infty,s=1..tr}=\widehat{Y}_{0,tr=1..tr}\hat{\theta}^{\infty}_{d=1..DOF,s=1..tr}. \tag{10}$$

Several attempts were made to predict the initial PpIX ratio in Y_0 from the dynamic parameters of the trajectory in $\hat{\theta}$. These attempts included biased hyperplane predictions using all coefficients in the dynamic model. Although the process is described by several dynamic states, the single exponential half life time was visualized briefly with respect to excitation power and initial conditions. This half life time is defined as the time from $t = 0$ for a component to reach the mean of the initial quantity and the converged quantity.

3. Results and Discussion

The eigenvalues in the diagonal matrix Σ, which was obtained from the SVD, revealed that all 40 891 spectra could be described by just four base spectra [see Fig. 3(a)]. The fourth base spectrum was classified as spiky residuals from background lighting, which only occur in the continuous wave (CW) mode when there is no dark subtraction. The fifth to tenth components are electronic readout noise, fast sinus, and cosines in the entire spectrum, independent of light intensities, that also cover the area below the long-pass fluorescent filter. These electronic reflections or read out errors can also be observed in a logarithmic frequency domain power plot of the entire data.

The measurements were projected onto the three spectral components. For the components to be meaningful, the coordinate system was rotated as follows. The angles of the first rotation were determined in such a way that the first spectral component minimizes the residuals with respect to the mean spectrum for all non-ALA-treated measurements; this component is denoted tissue autofluorescence. The angles of the second rotation are found by maximizing the variance from 627 nm to 642 nm in the second component and is denoted PpIX. The remaining component is referred to as a blue-shift of the autofluorescence [see Fig. 3(b)]. Further, data were also projected on the spiky background residual from the CW mode and a flat bias. These two last-mentioned

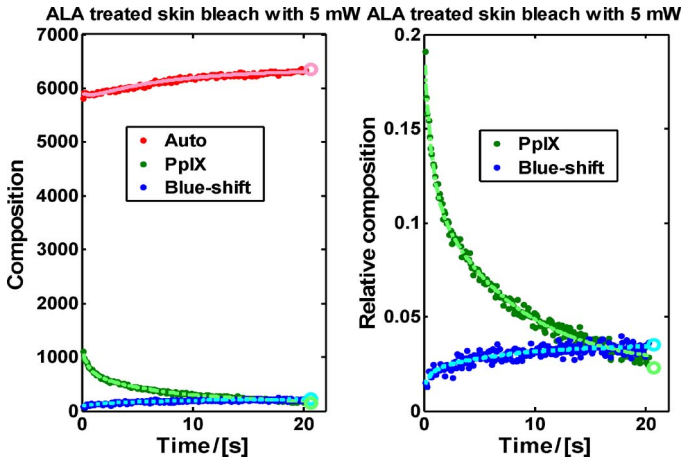

Fig. 4. Results for ALA-treated skin bleached with a power of 5 mW. (Left) Absolute fluorescence intensity expressed as counts as a function of time. In this particular sequence, the autofluorescence increases. (Right) Dimensionless values of the concentrations of PpIX and the blue-shift obtained by dividing them with the autofluorescence. The circles indicate convergence of each component; note that the convergence for the PpIX ratio is significantly different from zero. This particular sequence was recorded in continuous mode.

projections were later removed from data. Compression sequence residuals $(M - \widehat{M})$ were analyzed in the spectral domain and in the measurements from different individuals, and no systematic errors were found. The squared compression residuals were also analyzed in logarithmic histograms; obviously, sequences acquired at lower excitation power yielded larger relative residuals due to noise.

When the skin data are projected on the base components the composition can be plotted as a function of time [see Fig. 4(a)]. In this particular case, the autofluorescence increases slightly during bleaching. The average relative change in autofluorescence was not significant, being 0% for ALA-treated and -2% for nontreated tissue, both with standard deviations of 8%. The large variance from sequence-to-sequence implies that some sequences show a relative change as large as $\pm 20\%$. ALA-treated tissue showed a weak significant negative power dependence of 0.4%/mW relative change, whereas nontreated tissue showed no power dependence. To convert the fluorescence intensity in terms of counts into normalized quantities related to concentration, the PpIX and the blue-shift counts were divided by the with autofluorescence counts [see Fig. 4(b)]. This operation cancels out several aspects related to the geometry of the interrogation volume. This operation can be compared with standard dimensionless evaluation methods in computer vision [50] or spectroscopy where, e.g., the Raman signal from water or nitrogen matrices is used for normalization [51], [52]. Tissue autofluorescence is arguably more arbitrary due to the complexity of the tissue matrix; however, in our data set, all the interrogation volumes could be described by the three components in Fig. 3(b).

We describe the evolution of the ratios by a 6-DOF model, as described above, and two initial conditions: $PpIX_0$ and $BlueShift_0$

$$\widehat{C}_{t+1,s=1..2} = [1 \quad \widehat{C}_{t,s=1..2}]\hat{\theta}_{d=1..3,s=1..2}. \tag{11}$$

It was noted that even the absolute values at any time can be reconstructed from a linear combination of these two time series. Thus, there are only two dynamic states, although three base spectra were found; this is in accordance with previous findings [23], [24], [37]. We refer to these dynamic states as the "PpIX ratio" and "Blue-shift ratio," respectively. Models which did not converge, or models which converged but contained complex eigenvalues, were omitted, leaving 191 of 219 sequences. Several of the omitted sequences were short and noisy, and some were discontinuous due to movement during the measurement. In some of the sequences, fast periodic

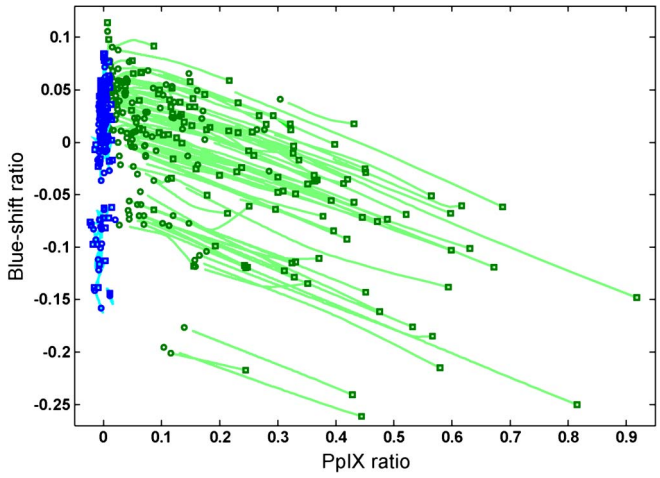

Fig. 5. Map of trajectories in state space. Squares indicate starting points, and circles are infinity extrapolated by solving for the derivative equaling zero. Green lines represent sequences from ALA-treated skin sample, and blue lines represent non ALA-treated sequences.

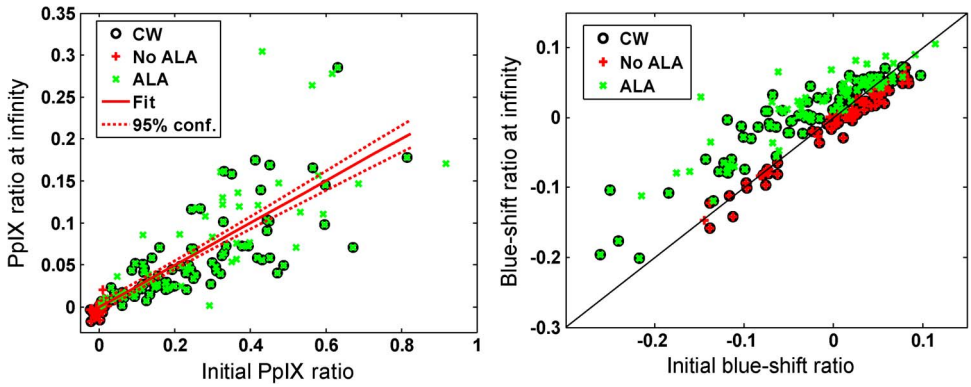

Fig. 6. (Left) The correlation between initial PpIX ratios and infinity extrapolated ratios is 0.83 (p-value 10^{-50}). This is promising with regard to estimating initial concentrations in terms of the constant infinity extrapolated properties. Green: ALA-treated tissue. Red: Nontreated tissue. Circles: Instrument operated in CW without dark subtraction. Crosses: Instrument operated in modulated mode. (Right) Infinite blue-shift ratio versus the initial blue-shift ratio. Green: ALA-treated sample. Red: Nontreated sample. Circles: Instrument operated in CW without dark subtraction. Initially, ALA-treated skin has lower blue-shift ratio than nontreated skin. After bleaching to infinity, ALA-treated skin has a higher blue-shift ratio than nontreated skin.

residuals were observed in the regime of heart beat frequency. Other slow time-dependent behaviors could arise from breathing [43], [44]. No systematic differences were found between the residuals and the squared residuals with respect to the early and late measurement points.

Considering the relative compositions of PpIX and blue-shift ratios, the state space trajectories can be mapped out in a plane, as illustrated in Fig. 5. It can be seen that the convergence points for ALA-treated samples (indicated by circles) are not located at a PpIX ratio of zero.

If we assume that each sequence starts with an entirely unbleached interrogation volume, we can plot the initial ratio of PpIX versus the ratio at infinity [see Fig. 6(a)]. The correlation coefficient was $r = 0.83$ (p-value 10^{-50}). For the convenience of the reader, a straight line was fitted (slope 0.25 $\pm$ 0.024 PpIX Inf/Init and intercept -0.00031 ± 0.0065 PpIX Inf, confidence 95%). The confidence interval is for the line fit. As can be seen from Fig. 6(a), confidence for new observation is dependent

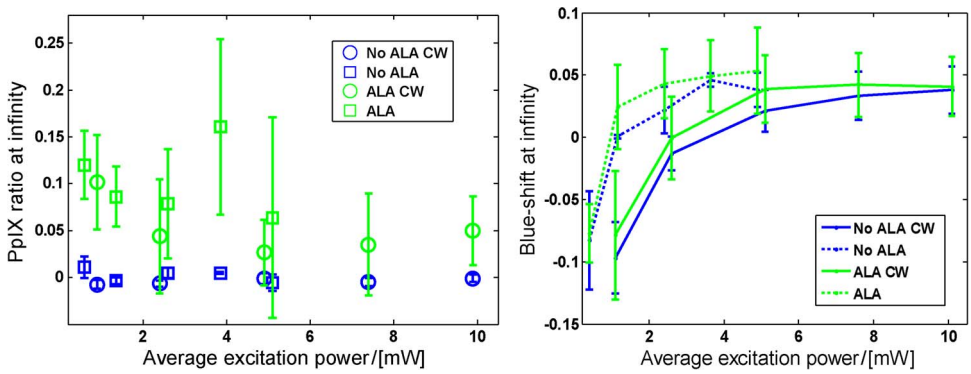

Fig. 7. (Left) PpIX ratio convergence is invariant with respect to excitation power. No significant difference between pulsed or CW. (Right) Higher excitation yields bluer convergence points. No significant difference between pulsed or CW, ALA, or no ALA.

on the initial value. Since the convergence point is independent of bleaching, this shows that the convergence point could potentially be used for bleaching-insensitive clinical evaluation.

We investigated whether the prediction of the initial PpIX ratio could be further improved by including the remaining parameters such as blue-shift convergence or decay times. These attempts included multivariate polynomial prediction models, which also include cross-product terms. No significant improvement was observed. We investigated the results in Fig. 6 in relation to whether the absolute autofluorescence increases or diminishes during bleaching, and no relation was found. When analyzing the blue-shift component in a similar manner, we observed that the blue-shift of ALA-treated tissue increased with bleaching, whereas nontreated tissue showed a slight red-shift [see Fig. 6(b)]. For the two aforementioned analyses, no systematic difference between the individuals was found.

To investigate whether the nonzero convergence concentration of PpIX arises from its production or in-flow in the interrogation volume, or whether it arises from PpIX trapped in the cell organelles, with inhibiting bleaching due to the low dissolved oxygen concentrations, we performed an excitation power analysis. Fig. 7(a) shows the PpIX ratio at infinity in relation to bleaching power. No significant power dependence could be seen. At very lower excitation powers, a slight increase in PpIX ratio convergence is observed, but this could equally well be explained by the noisy conditions. When applying the same analysis to the blue-shift ratio [see Fig. 7(b)], we observed that higher excitation powers yielded convergence points with a higher blue-shift. Similar results were obtained in [53].

No significant relation was found between the dynamic coefficients in the system matrix, i.e., the decay rates, and the initial PpIX ratio (in accordance with previous findings [23]). When performing excitation power analysis on the half life time of PpIX ratio, we observed a rather large variance between the different sequences. If we assume that the fluorescence bleaching half life time depends on the power according to $t_{1/2} = k_0 + k_1/P$ (k_0 implies constraints on the bleaching other than excitation flux), we observe that the decay rates saturates within the range of excitation powers used in clinical situations, which is typically 5 mW (see Fig. 8). This would suggest that in-flow of oxygen into the interrogation volume constrains the bleaching process, rather than excitation flux [18]. One considerable difference between continuous and modulated bleaching is the in-flow of, e.g., PpIX and oxygen during the dark time slots.

Several bleaching sequences from an open brain surgery situation were analyzed using SVD analysis, as described above. The eigenvalues revealed that spectra in the sequences could be effectively described by four base spectra; however, each sequence only required two components, namely, tissue autofluorescence and the PpIX signal. When rotating the coordinate system to minimize the PpIX imprint on the autofluorescence, the following two observations were made: The PpIX peak wavelength was slightly higher than for the skin (637 nm versus 634 nm for skin), and there was a change of the spectral knee shape in the region 650–700 associated with

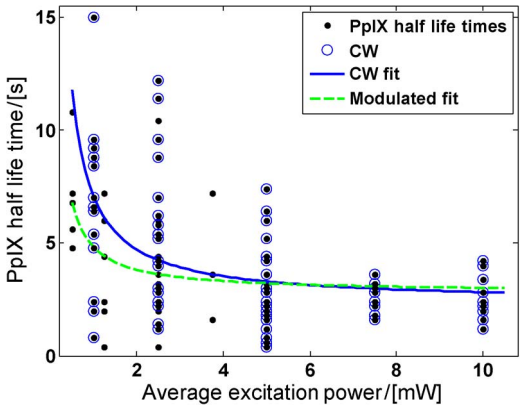

Fig. 8. Half life time of the PpIX ratio from the initial value to the final value. The data were fitted with the function $t_{1/2} = k_0 + k_1/P$. Such bottleneck behavior suggests that bleaching is limited by oxygen diffusion once the excitation light flux saturates.

TABLE 1

For short sequence lengths, noise and small bleaching degree are reflected in the 95% confidence bounds

Mode	PpIX ratio @ t=0	PpIX ratio @ t=inf	PpIX half life time / [s]
CW, 5mW	1.39 [1.37…1.40]	0.156 [-1.27…1.576]	48.69 [-16.23…113.6]
CW, 5mW	2.61 [2.58…2.64]	1.058 [-0.16…2.27]	71.1 [0.94…141.3]
CW, 5mW	2.24 [2.22…2.26]	0.713 [0.60…0.83]	18.27 [15.94…20.61]
Modulated, 2.5mW	1.53 [1.50…1.56]	0.403 [0.35…0.46]	12.63 [11.23…14.03]
Modulated, 2.5mW	1.39 [1.36-1.43]	0.530 [0.47...0.58]	6.964 [5.82...8.11]

photoproducts of PpIX [40]. A possible explanation for the shift could be different instrument temperatures or different scattering properties [54]. However, in continuous mode, it is difficult to distinguish this knee from the migrated red light from neighboring regions induced by the strong surgery theater lamp. The plurality of spectral components needed for the three different sequences on *in vivo* brain samples are mainly assigned different background conditions, as well as small spectral shifts of the PpIX signal in the order of 2 nm.

The temporal evolution of the PpIX ratio was in this case effectively explained by a single exponential with a bias or a state space model of the form

$$C_{t=1..T,s=1} = [1 \quad C_{t=0..T-1,s=1}]\theta_{d=1..2}. \tag{12}$$

One reason for this could be the fact that the strong theater lamp would induce a considerable bleaching of any fast bleaching component before the sequence could be recorded.

The magnitudes of the base components have been scaled to match those given above in this paper [see Fig. 3(b)], and thus, we can compare the convergence PpIX ratios directly. The details of the brain sequences are given in Table 1. We note that the convergence PpIX ratio is relatively high compared with those presented in, e.g., Fig. 6(a) (especially for the values with the better confidence intervals). This could be an indication of the applicability of the method presented, since the sequences of the brain samples were all measured on changes.

Fig. 9 presents an initial and a converged spectra. It should be noted that the interrogation volume is likely to have undergone bleaching prior to the recording due to the operating theater lamp.

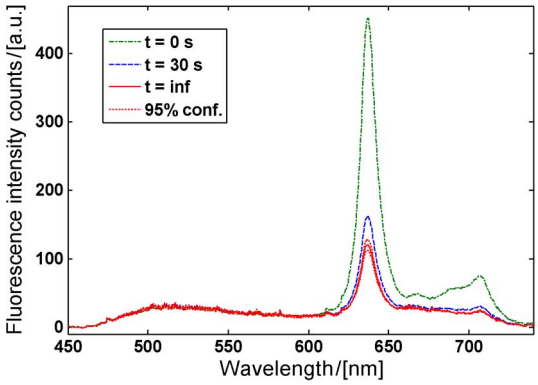

Fig. 9. Initial and infinity spectrum from an *in vivo* brain bleaching sequence.

There were no indications of PpIX bleaching photoproducts in the skin data, while the blue-shift increased during bleaching. However, bleaching features changing the spectral shape in the 650–700-nm range were observed in brain tissue (see Fig. 9). The photoproduct from PpIX bleaching has been observed previously in skin samples [22], [38]; one possible explanation is the difference that, in this paper, healthy skin was studied, whereas malignant skin was studied in [38]. Interestingly, the production of the photoproducts is dynamically locked to the destruction of PpIX; thus, PpIX and photoproducts will not be separated by the SVD analysis of a bleaching sequence; instead, the SVD will e.g., express a steady spectral component and a component representing both the reduction of PpIX and the increase in the photoproducts.

4. Conclusion

Using data from ALA-treated and non-ALA-treated skin and brain tissue *in vivo*, we have shown that bleaching sequences from individual interrogation volumes can be effectively described by a small number of spectral components (three and two, respectively). We have also shown that we can accurately predict the spectra in time and extrapolate them to infinity. We observed an interesting correlation between the PpIX ratio after infinite bleaching and the initial PpIX ratio (related to the respective concentrations). In a clinical situation, this would allow us to obtain bleaching-insensitive quantities by recording short sequences instead of individual spectra. Within the power regime 0.35–3.5 W/cm^2, the PpIX convergence ratio is independent of power, which indicates that the converged PpIX signal probably arises from organelles where oxygenation inhibits bleaching, rather than the in-flow or production of PpIX. A large spread in the bleaching half life times was observed; the PpIX half life time was found to be unrelated to the initial PpIX concentration. This is encouraging since the convergence point is easier to determine, whereas a half life time can only be determined for the limited time during which the sequence shows any significant bleaching.

The instrument used in this paper features a large number of spectral bands but rather low optical throughput and sampling frequency. The fact that the large data set can be described by very few spectral components suggests that sensitivity and modulation speed should be prioritized in future instruments at the expense of spectral resolution. This would greatly increase the signal-to-noise and signal-to-background (operating theater lamp) ratio. A second generation instrument is likely to be based on a set of dichroic beam splitters [16] and photomultiplier tubes (PMTs) or avalanche photodiodes (APDs), which would enable modulation in the kilohertz regime and compatibility with fluorescence lifetime acquisition [55]. It is well known that the fluorescence is largely influenced by re-absorption; thus, it is desirable to include a white light source for elastic reflectance, e.g., an InGaN+Ce:YAG LED [56]. Such a feature may further improve the prediction of the initial PpIX content and reduce some of the biological variance between different interrogation volumes caused by, e.g., re-absorbing chromophores and, not least, the different local oxygen levels (accessed by the absorbance of Hb and HbO). In this paper, the elastic scattered excitation light was rejected by

a long-pass filter. Detailed information on the change of the extension of the interrogation volume could be obtained by even considering the elastically scattered excitation light. We have shown how certain properties can be investigated by analyzing the bleaching dynamics with respect to the excitation power [39]; in this paper, the different powers were applied to different interrogation volumes. In future studies, it could be interesting to bleach the same interrogation volume by a plurality of excitation powers to investigate the properties related to intraorganellular PpIX, the diffusion of oxygen, and production and diffusion of PpIX.

Acknowledgment

The authors acknowledge Prof. S. Svanberg for his valuable input. We also thank J. Richter, a neurosurgeon with the Department of Neurosurgery, Linköping University, for the opportunity to conduct measurements during surgeries. We also thank R. Johansson for his efforts related to the dynamical modeling.

References

[1] M. A. Mycek and B. W. Pogue, Eds., *Handbook of Biomedical Fluorescence*. Boca Raton, FL: CRC, 2003, p. 688.
[2] J. Moan and Q. Peng, "An outline of the history of PDT," in *Photodynamic Therapy*, T. Patrice, Ed. Cambridge, U.K.: Roy. Soc. Chem., 2003, pp. 1–18.
[3] C. af Klinteberg, "On the use of light for the characterization and treatment of malignant tumours," Ph.D. dissertation, Lund Univ., Lund, Sweden, 1999.
[4] J. Moan, J. T. H. M. Van Den Akker, P. Juzenas, L. W. Ma, E. Angell-Petersen, Ø. B. Gasmar, and V. Iani, "On the basis for tumor selectivity in the 5-aminolevulinic acid-induced synthesis of protoporphyrin IX," *J. Porphyr. Phthalocya.*, vol. 5, no. 2, pp. 170–176, Feb. 2001.
[5] A. Novotny and W. Stummer, "5-Aminolevulinic acid and the blood-brain barrier—A review," *Med. Laser Appl.*, vol. 18, no. 1, pp. 36–40, 2003.
[6] W. Stummer, U. Pichlmeier, T. Mainel, O. D. Wiestler, F. Zanella, and H. Reulen, "Fluorescence-guided surgery with 5-aminolevulinic acid for resection of malignant glioma: A randomized controlled multicentre phase III trial," *Lancet Oncol.*, vol. 7, no. 5, pp. 392–401, May 2006.
[7] S. Utsuki, H. Oka, S. Sato, S. Shimizu, S. Suzuki, Y. Tanizaki, K. Kondo, Y. Miyajima, and K. Fujii, "Histological examination of false positive tissue resection using 5-aminolevulinic acid-induced fluorescence guidance," *Neurol. Med. Chir. (Tokyo)*, vol. 47, no. 5, pp. 210–214, May 2007.
[8] B. W. Pogue, S. L. Gibbs-Strauss, P. A. Valdés, K. S. Samkoe, D. W. Roberts, and K. D. Paulsen, "Review of neurosurgical fluorescence imaging methodologies," *IEEE J. Sel. Topics Quantum Electron.*, vol. 16, no. 3, pp. 493–505, May/Jun. 2010.
[9] M. Hefti, G. von Campe, A. Siegner, H. Looser, and H. Landolt, "5-Aminolaevulinic acid-induced protoporphyrin IX fluorescence in high-grade glioma surgery," *Swiss Med. Wkly.*, vol. 138, no. 11/12, pp. 180–185, Mar. 2008.
[10] M. A. Scott, C. Hopper, A. Sahota, R. Springett, B. W. McIlroy, S. G. Bown, and A. J. MacRobert, "Fluorescence photodiagnostics and photobleaching studies of cancerous lesions using ratio imaging and spectroscopic techniques," *Lasers Med. Sci.*, vol. 15, no. 1, pp. 63–72, 2000.
[11] C. af Klinteberg, M. Andreasson, O. Sandström, S. Andersson-Engels, and S. Svanberg, "Compact medical fluorosensor for minimally invasive tissue characterization," *Rev. Sci. Instrum.*, vol. 76, no. 3, p. 034303, Mar. 2005.
[12] M. A. Ilias, J. Richter, F. Westermark, M. Brantmark, S. Anderson-Engels, and K. Wårdell, "Evaluation of a fiber-optic fluorescence spectroscopy system to assist neurosurgical tumor resections," *Proc. SPIE*, vol. 6631, pp. 66310W-1–66310W-8, 2007.
[13] N. Haj-Hosseini, J. Richter, S. Andersson-Engels, and K. Wårdell, "Optical touch pointer for fluorescence guided glioblastoma resection using 5-aminolevulinic acid," *Lasers Surg. Med.*, vol. 42, no. 1, pp. 9–14, Jan. 2010.
[14] J. Richter, N. Haj-Hosseini, S. Anderson-Engels, and K. Wårdell, "Fluorescence spectroscopy measurements in ultrasonic navigated resection of malignant brain tumors," *Lasers Surg. Med.*, vol. 43, no. 1, pp. 8–14, Jan. 2011.
[15] I. A. Boere, D. J. Robinson, H. S. de Bruijn, J. Boogert, H. W. Tilanus, H. J. C. M. Sterenborg, and R. W. F. de Bruin, "Monitoring in situ dosimetry and protoporphyrin IX fluorescence photobleaching in the normal rat esophagus during 5-aminolevulinic acid photodynamic therapy," *Photochem. Photobiol.*, vol. 78, no. 3, pp. 271–277, Sep. 2003.
[16] B. W. Pogue, C. Sheng, X. Zhou, P. Hoopes, and T. Hasan, "Photobleaching-based dosimetry predicts deposited dose in ALA-PpIX PDT of rodent esophagus," *Photochem. Photobiol.*, vol. 83, no. 3, pp. 738–748, May/Jun. 2007.
[17] N. Haj-Hosseini, J. Richter, S. Andersson-Engels, and K. Wårdell, "Photobleaching behavior of protoporphyrin IX during 5-aminolevulinic acid marked glioblastoma detection," *Proc. SPIE*, vol. 7161, p. 716131, 2009.
[18] A. Curnow, B. W. McIlroy, M. J. Postle-Hacon, A. J. MacRobert, and S. G. Bown, "Light dose fractionation to enhance photodynamic therapy using 5-aminolevulinic acid in the normal rat colon," *Photochem. Photobiol.*, vol. 69, no. 1, pp. 71–76, Jan. 1999.
[19] J. Moan, L. Ma, V. Iani, and A. Juzeniene, "Influence of light exposure on the kinetics of protoporphyrin IX formation in normal skin of hairless mice after application of 5-aminolevulinic acid methyl ester," *J. Invest. Dermatol.*, vol. 125, no. 5, pp. 1039–1044, Nov. 2005.
[20] K. K. Wang, S. Mitra, and T. H. Foster, "A comprehensive mathematical model of microscopic dose deposition in photodynamic therapy," *Med. Phys.*, vol. 34, no. 1, pp. 282–293, Jan. 2007.

[21] A. Orenstein, G. Kostenich, and Z. Malik, "The kinetics of protoporphyrin fluorescence during ALA-PDT in human malignant skin tumors," *Cancer Lett.*, vol. 120, no. 2, pp. 229–234, Dec. 1997.
[22] J. C. Finlay, D. L. Conover, E. L. Hull, and T. H. Foster, "Porphyrin bleaching and PDT-induced spectral changes are irradiance dependent in ALA-sensitized normal rat skin *in vivo*," *Photochem. Photobiol.*, vol. 73, no. 1, pp. 54–63, Jan. 2001.
[23] D. J. Robinson, H. S. de Bruijn, N. van der Veen, M. R. Stringer, S. B. Brown, and W. M. Star, "Fluorescence photobleaching of ALA-induced protoporphyrin IX during photodynamic therapy of normal hairless mouse skin: The effect of light dose and irradiance and the resulting biological effect," *Photochem. Photobiol.*, vol. 67, no. 1, pp. 140–149, Jan. 1998.
[24] A. Lihachev and J. Spigulis, "Skin autofluorescence fading at 405/532 nm laser excitation," *IEEE Xplore,* 10.1109/NO, vol. 10, pp. 63–65, 2007.
[25] T. W. Anderson, *An Introduction to Multivariate Statistical Analysis,* 3rd ed. Hoboken, NJ: Wiley, 2003.
[26] A. C. Rechner, *Methods of Multivariate Analysis*. New York: Wiley Interscience, 2002.
[27] K. R. Beebe and B. R. Kowalski, "An introduction to multivariate calibration and analysis," *Anal. Chem.*, vol. 59, pp. 1007A–1017A, 1987.
[28] P. Weibring, T. Johansson, H. Edner, S. Svanberg, B. Sundnér, V. Raimondi, G. Cecchi, and L. Pantani, "Fluorescence lidar imaging of historical monuments," *Appl. Opt.*, vol. 40, no. 33, pp. 6111–6120, Nov. 2001.
[29] P. Weibring, T. Johansson, H. Edner, S. Svanberg, B. Sundnér, V. Raimondi, G. Cecchi, and L. Pantani, "Fluorescence lidar imaging of historical monuments: Erratum," *Appl. Opt.*, vol. 41, no. 3, pp. 434–436, Jan. 2002.
[30] MATLAB, Help files, The Mathworks.
[31] L. Ljung, *System Identification: Theory for the User,* 2nd ed. Englewood Cliffs, NJ: Prentice-Hall, 1999, 672 p.
[32] R. Isermann, *Identification of Dynamical Systems: An Introduction With Applications,* 1st ed. New York: Springer-Verlag, 2010, p. 550.
[33] Y. Zhu, *Multivariable System Identification for Process Control,* 1st ed. Amsterdam, The Netherlands: Elsevier, 2001, 372 p.
[34] R. Johansson, *System Modeling and Identification*. Englewood Cliffs, NJ: Prentice-Hall, 1993, p. 528.
[35] S. Bittanti and G. Picci, Eds., *Identification, Adaptation, Learning: The Science of Learning Models from Data (NATO ASI Series/Computer and Systems Sciences),* 1st ed. New York: Springer-Verlag, 1996, 552 p.
[36] S. Dobre, T. Bastogne, M. Barberi-Heyob, D. Bechet, J. Didelon, and A. Richard, "System identification of the intracellular photoreaction process induced by photodynamic therapy," in *Proc. 16th Mediterranean Conf. Control Autom.*, Ajaccio, France, Jun. 2008, pp. 1729–1734.
[37] J. C. Finlay, S. Mitra, M. S. Patterson, and T. H. Foster, "Photobleaching kinetics of Photofrin *in vivo* and in multicell tumour spheroids indicate two simultaneous bleaching mechanisms," *Phys. Med. Biol.*, vol. 49, no. 21, pp. 4837–4860, Nov. 2004.
[38] C. af Klinteberg, A. M. K. Enejder, I. Wang, S. Andersson-Engels, S. Svanberg, and K. Svanberg, "Kinetic fluorescence studies of 5-aminolaevulinic acid-induced protoporphyrin IX accumulation in basal cell carcinomas," *J. Photochem. Photobiol. B: Biol.*, vol. 49, no. 2/3, pp. 120–128, Apr. 1999.
[39] K. K. Wang, W. J. Cottrell, S. Mitra, A. R. Oseroff, and T. H. Foster, "Simulations of measured photobleaching kinetics in human basal cell carcinomas suggest blood flow reductions during ALA-PDT," *Lasers Surg. Med.*, vol. 41, no. 9, pp. 686–696, Nov. 2009.
[40] W. J. Cottrell, A. D. Paquette, K. R. Keymel, T. H. Foster, and A. R. Oseroff, "Irradiance-dependent photobleaching and pain in delta-aminolevulinic acid-photodynamic therapy of superficial basal cell carcinomas," *Clin. Cancer Res.*, vol. 14, no. 14, pp. 4475–4483, Jul. 2008.
[41] B. W. Pogue, C. Sheng, J. Benevides, D. Forcione, B. Puricelli, N. Nishioka, and T. Hasan, "Protoporphyrin IX fluorescence photobleaching increases with the use of fractionated irradiation in the esophagus," *J. Biomed. Opt.*, vol. 13, no. 3, p. 034009, May/Jun. 2008.
[42] J. S. Dysart and M. S. Pattersson, "Photobleaching kinetics, photoproduct formation, and dose estimation during ALA induced PpIX PDT of MLL cells under well oxygenated and hypoxic conditions," *Photochem. Photobiol. Sci.*, vol. 5, no. 1, pp. 73–81, 2006.
[43] J. Spigulis, "Optical non-invasive monitoring of skin blood pulsations," *Appl. Opt.*, vol. 44, no. 10, pp. 1850–1857, Apr. 2005.
[44] J. Spigulis, L. Gailite, A. Lihachev, and R. Erts, "Simultaneous recording of skin blood pulsations at different vascular depths by multi-wavelength photoplethysmography," *Appl. Opt.*, vol. 46, no. 10, pp. 1754–1759, Apr. 2007.
[45] H. Heyerdahl, I. Wang, D. L. Liu, R. Berg, S. Anderson-Engels, Q. Peng, J. Moan, S. Svanberg, and K. Svanberg, "Pharmacokinetic studies on 5-aminolevulinic acid-induced protoporphyrin IX accumulation in tumours and normal tissues," *Cancer Lett.*, vol. 112, no. 2, pp. 225–231, Jan. 1997.
[46] N. van der Veen, H. S. de Bruijn, R. J. W. Berg, and W. M. Star, "Kinetics and localisation of PpIX fluorescence after topical and systemic ALA application, observed in skin and skin tumours of UVB-treated mice," *Brit. J. Cancer*, vol. 73, no. 7, pp. 925–930, Apr. 1996.
[47] M. Shirmanova, E. Zagaynova, M. Sirotkina, L. Snopova, I. Balalaeva, I. Krutova, N. Lekanova, I. Turchin, A. Orlova, and M. Kleshnin, "*In vivo* study of photosensitizer pharmacokinetics fluorescence transillumination imaging," *J. Biomed. Opt.*, vol. 15, no. 4, p. 048004, Jul./Aug. 2010.
[48] J. Johansson, R. Berg, K. Svanberg, and S. Svanberg, "Laser-induced fluorescence studies of normal and malignant tumour tissue of rat following intravenous injection of δ-amino levulinic acid," *Lasers Surg. Med.*, vol. 20, no. 3, pp. 272–279, 1997.
[49] B. Kramer and K. Uberriegler, "*In-vitro* investigation of ALA-induced protoporphyrin IX," *J. Photochem. Photobiol. B: Biol.*, vol. 36, no. 2, pp. 121–126, Nov. 1996.
[50] M. Drew and J. Au, "Clustering of compressed illumination-invariant chromaticity signatures for efficient video summarization," *Image Vis. Comput.*, vol. 21, no. 8, pp. 705–716, Aug. 2003.

[51] F. E. Hoge and R. N. Swift, "Airborne simultaneous spectroscopic detection of laser-induced water Raman backscatter and fluorescence from chlorophyll a and other naturally occurring pigments," *Appl. Opt.*, vol. 20, no. 18, pp. 3197–3205, Sep. 1981.
[52] D. N. Whiteman, S. H. Melfi, and R. A. Ferrare, "Raman LIDAR system for the measurement of water-vapor and aerosols in the Earth's atmosphere," *Appl. Opt.*, vol. 31, no. 16, pp. 3068–3082, Jun. 1992.
[53] B. W. Pogue, J. D. Pitts, M. A. Mycek, R. D. Sloboda, C. M. Wilmot, J. F. Brandsema, and J. A. O'Hara, "*In vivo* NADH fluorescence monitoring as an assay for cellular damage in photodynamic therapy," *Photochem. Photobiol.*, vol. 74, no. 6, pp. 817–824, Dec. 2001.
[54] J. Swartling, J. Svensson, D. Bengtsson, K. Terike, and S. Andersson-Engels, "Fluorescence spectra provide information on the depth of fluorescent lesions in tissue," *Appl. Opt.*, vol. 44, no. 10, pp. 1934–1941, Apr. 2005.
[55] P. V. Butte, A. N. Mamelak, M. Nuno, S. I. Bannykh, K. L. Black, and L. Marcu, "Fluorescence lifetime spectroscopy for guided therapy of brain tumors," *NeuroImage (IBMISPS)*, vol. 54, pp. 125–135, 2011.
[56] M. Brydegaard, P. Lundin, Z. Guan, A. Runemark, S. Åkesson, and S. Svanberg, "Feasibility study: Fluorescence lidar for remote bird classification," *Appl. Opt.*, vol. 49, no. 24, pp. 4531–4544, Aug. 2010.